

pubs.acs.org/JAFC Article

Evaluation of Cell Wall Chemistry of Della and Its Mutant Sweet Sorghum Stalks

Endalkachew Mengistie, Abdulbaset M. Alayat, Farid Sotoudehnia, Norbert Bokros, Seth DeBolt, and Armando G. McDonald*



Cite This: J. Agric. Food Chem. 2022, 70, 1689–1703



ACCESS

Metrics & More

Article Recommendations

Supporting Information

ABSTRACT: The cell wall compositional (lignin and polysaccharides) variation of two sweet sorghum varieties, Della (D) and its variant *REDforGREEN* (RG), was evaluated at internodes (IN) and nodes (N) using high-performance liquid chromatography (HPLC), pyrolysis—gas chromatography-mass spectrometry (Py-GCMS), X-ray diffraction (XRD), and two-dimensional (2D) 1 H $^{-13}$ C nuclear magnetic resonance (NMR). The stalks were grown in 2018 (D1 and RG1) and 2019 (D2 and RG2) seasons. In RG1, Klason lignin reductions by 16–44 and 2–26% were detected in IN and N, respectively. The analyses also revealed that lignin from the sorghum stalks was enriched in guaiacyl units and the syringyl/guaiacyl ratio was increased in RG1 and RG2, respectively, by 96% and more than 2-fold at IN and 61 and 23% at N. The glucan content was reduced by 23–27% for RG1 and by 17–22% for RG2 at internodes. Structural variations due to changes in both cellulose- and hemicellulose-based sugars were detected. The nonacylated and γ-acylated β $^-$ O $^-$ 4 linkages were the main interunit linkages detected in lignin. These results indicate compositional variation of stalks due to the RG variation, and the growing season could influence their mechanical and lodging behavior.

KEYWORDS: sorghum, nodes, internodes, lignin, cellulose, 2D-NMR

1. INTRODUCTION

Sorghum is a versatile grass grown for grain, sugar, forage, and bioenergy applications. Stalks of sorghums are load-bearing frameworks providing mechanical support to the aboveground shoot components.² Sorghum is one of the main crops that is highly affected by lodging. Lodging, the structural instability and failure of the stalk to support the shoot components before maturity and harvesting, is a major agronomic challenge leading to considerable yield losses, grain-quality reductions, and an increase in the cost of harvesting.3 It has been predicted that lodging-induced yield losses can reach up to 60% in some crops. One of the strategies of enhancing lodging resistance is by developing varieties having resilient mechanical property of cell walls, which plays an important role in defining the stalk strength. Especially in high-yield sorghums (having a greater load on the stem), strong mechanical properties of plant cell walls are vital to avoid product loss due to stalk lodging.

Plant cell wall structures are three-dimensional networks composed of primarily cellulose, hemicellulose, and lignin. So Cell walls have different compositional, rheological, and mechanical properties and provide strength, maintain rigidity, and protect the cell structural integrity. Their composition mainly depends on the amount and distribution of constituents along the different anatomical features of the stalks. Plant cell walls are further divided into primary and secondary walls. Primary cell walls are thinner and more flexible structures surrounding growing cells, mainly composed of cellulose, pectin, and xyloglucans with lesser amounts of arabinoxylans and structural proteins. Secondary cell walls are more rigid and stronger than primary cell walls, comprising cellulose, lignin, xylan, and glucomannan. The composition and the

chemistry of the plant cell wall affect the mechanical behavior of the stalk. 9

Stalk lodging is a multidimensional phenomenon dependent on cell wall compositions, stalk morphology, anatomical and metrological factors, biological factors, soil type, and inorganic nutrients. 10,11 Previously published literature has shown that the stalk lodging incidence is highly related to the bending strength of the stalks, 10 which suggests that the biomechanical properties of stalks largely determine their lodging resistance. Lignin, which is one of the major structural components of secondary cell walls, enhances plant growth and lodging resistance of the cell wall.¹² Furthermore, lignin plays an important role in cementing cellulose and hemicelluloses within the cell walls, thus aiding in improving the integrity and mechanical strength of the stalk. Lignin content was shown to be closely related to the lodging resistance behavior of the stem. Studies have shown that a low lignin content in crops resulted in weak mechanical strength of the stem. 13

On the other hand, the application of sorghum for lignocellulosic biomass utilization has been highly limited by the recalcitrance of the cell wall, which is mainly attributed to lignin—carbohydrate complexes (LCCs) and rigid lignin. One of the promising approaches to mitigating cell wall recalcitrance and thereby improving sugar release and

Received: November 10, 2021 Revised: December 23, 2021 Accepted: January 12, 2022 Published: January 31, 2022





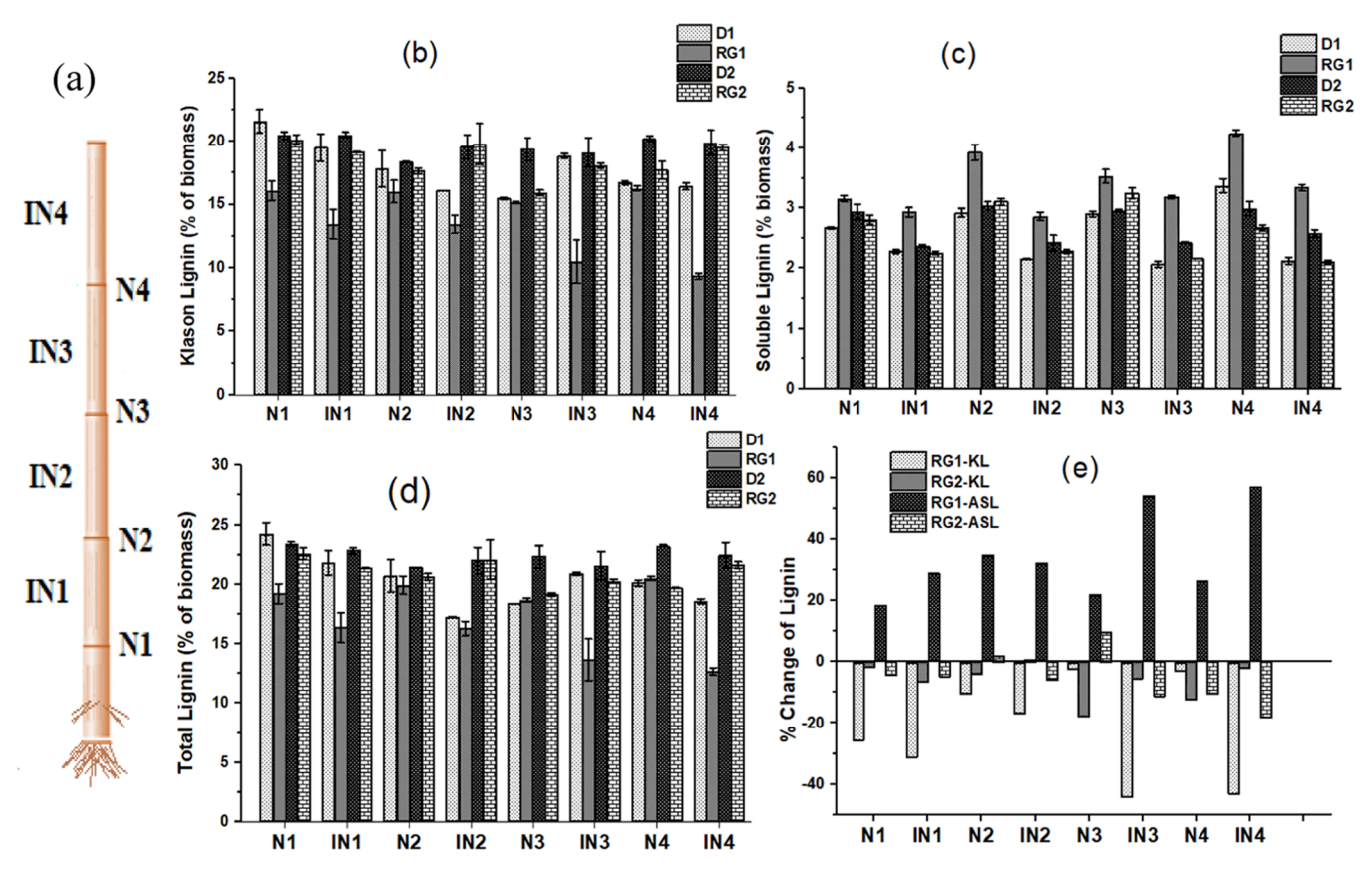


Figure 1. (a) Schematic depiction of sorghum stalk, (b) Klason lignin (KL), (c) acid-soluble lignin (ASL), (d) total lignin (TL), and (e) % change in ASL and KL for D1, RG1, D2, and RG2 sorghum stalks (% of biomass) at nodes (N) and internodes (IN).

digestibility of sorghum stalks is by reducing the lignin content through mutation, 15 which can be achieved by reducing the lignin content, modifying the lignin composition, or both.

Breeding has a prospect of producing easily digestible sweet sorghum varieties with altered chemistry. The REDforGREEN (RG) sorghum variety was developed through ethyl methane sulfonate (EMS) mutagenesis from the Della (D) variety and has shown an increase in digestibility. However, increased digestibility is typically associated with a lower stalk strength and a tendency for lodging. In relation to lodging, previous studies^{3,10,17} focused on macroscopic studies of stalk mechanical properties. Yet, understanding the biomechanical strength of stalks from the perspectives of their cell wall compositions is limited. Thus, for a comprehensive understanding of the cell wall composition across growing seasons and for the purpose of elucidating stalk biomechanical variations through chemical composition (which will be explored in future works), this study compares the cell wall composition of the RG mutant with its corresponding Della variety at the nodes (N) and internodes (IN) across two growing seasons.

2. MATERIALS AND METHODS

2.1. Plant Materials. Della (D) and RG sorghum varieties were grown in Lexington, KY, in 2018 (D1 and RG1) and 2019 (D2 and RG2). The compositional variations of the varieties across two growing seasons were evaluated. Samples of four to five matured stalks were pooled for each variety in both years and ground using a Thomas—Wiley mill. The moisture contents were determined using an HB43-S Halogen moisture analyzer (Mettler Toledo). The extractives were previously removed by Soxhlet extraction and analyzed, ¹⁸ and all subsequent structural carbohydrate analyses were

performed using extractive-free biomass in duplicates to ensure data reliability.

2.2. Lignin and Carbohydrate Analyses. Extractive-free biomass samples (200 mg), in duplicate, were hydrolyzed using sulfuric acid (2 mL, 72%) for 60 min at 30 °C in a water bath followed by secondary hydrolysis (4% sulfuric acid, 30 min, 20 psi) in an autoclave according to ASTM D 1106-96 with slight modifications. Klason lignin (KL) content was determined gravimetrically after filtration, whereas acid-soluble lignin (ASL) content was determined by UV spectroscopy (Genesys 50, ThermoScientific) at 205 nm¹⁹ using an absorption coefficient of 110 L g⁻¹ cm⁻¹. Structural carbohydrate component analysis was performed on the hydrolyzed filtrate (5 mL), with the addition of mannitol as an internal standard, according to ASTM E 1758-01. The sugars were separated and quantified using high-performance liquid chromatography (HPLC, two Rezex RPM columns in series, 7.8 mm × 300 mm, Phenomenex) at 85 °C on elution with water (0.5 mL min⁻¹) using differential refractive index detection (Waters model 2414).

2.3. Fourier Transform Infrared (FTIR) Spectroscopy. FTIR spectroscopy was performed on the biomass in triplicate using an iS5 spectrometer (Thermo-Nicolet) equipped with a ZnSe attenuated total reflection (iD5 ATR) accessory. The spectra were averaged, baseline-corrected, and normalized using Omnic v9 software. After spectral deconvolution using peak fitting, the syringyl/guaiacyl (S/G)²⁰ ratio was determined from the intensity ratio of 1325–1235 cm⁻¹, whereas the cellulose total crystallinity index (TCI) and lateral order index (LOI) were estimated, respectively, from the normalized intensity ratios of 1370-2920 cm⁻¹ $(I_{1370}/I_{2920})^{21}$ and 1427-898 cm⁻¹ $(I_{1427}/I_{898})^{22}$ As the TCI method was originally proposed for pure cellulose, the intensity of 1370 cm⁻¹ might be influenced by the neighboring bands when it is applied to the lignocellulosic sample.

2.4. Analytical Pyrolysis—Gas Chromatography-Mass Spectrometry (Py-GCMS) Analysis. The biomass S/G ratio was determined by pyrolysis—GCMS (Py-GCMS) using a Pyrojector II

unit (SGE Analytical Science) at 500 °C coupled to a GCMS (ISQ-Trace1300). The compounds were separated using a ZB-5 capillary column (30 m × 0.25 mm Ø, 0.25 μ m coating, Phenomenex) from 50 (1 min) to 250 °C (10 min) at 5 °C min⁻¹. Compounds were identified with authentic standards, by comparison with the literature^{23,24} and the NIST-2017 mass spectral library. p-Hydroxyphenyl/guaiacyl/syringyl (H/G/S) was determined from peak areas of lignin monomer pyrolyzates selected by an ion monitoring chromatogram for H between 7 and 15 min (m/z = 94, 107, 108, 120, 121, 134, 148), G between 18 and 23 min (m/z = 124, 135, 137, 138, 151, 164, 178), and S between 24 and 28 min (m/z = 154, 165, 167, 168, 181, 194, 208).²⁵

- **2.5. Thermogravimetric Analysis (TGA).** The thermal stability and decomposition behavior of the biomass samples were performed on a PerkinElmer TGA-7 instrument (5–6 mg, in triplicate) from 30 to 800 °C at 20 °C min⁻¹ under nitrogen (30 mL min⁻¹). The data were analyzed using Pyris v11 software.
- **2.6.** X-ray Diffraction (XRD). XRD analysis on biomass samples, in duplicate, was performed using a Siemens D5000 diffractometer using Cu K α radiation (λ = 0.154 nm) from 2θ = 2 to 80° at 0.05° steps. The crystallinity index (CI) of cellulose was determined after peak fitting methods were applied to the amorphous and crystalline [(1 $\overline{1}$ 0), (110), and (200)] regions of the diffractogram using two different methods: the deconvolution method (eq 1)²⁶ and the peak height method (eq 2).²⁷

$$CI_{d}(\%) = \left(\frac{\sum A_{cry}}{\sum A_{cry} + \sum A_{am}}\right) \times 100$$
(1)

$$CI_{h}$$
 (%) = $\left(\frac{I_{200} - I_{am}}{I_{200}}\right) \times 100$ (2)

where I_{200} and $I_{\rm am}$ are, respectively, the intensity of the main crystallite at (200) and amorphous. The mean width of crystallites of cellulose determines the broadness of XRD diffractograms and is inversely proportional to broadening. The size of the crystallite at the (200) plane was determined using the Scherrer formula in eq 3.²⁸

$$L = \frac{57.3k\lambda}{\beta\cos\theta} \tag{3}$$

Here, k is the shape factor of the crystal (0.91), λ is the wavelength of the X-ray, β is the full width at half-maximum (FWHM) of the crystalline peak, θ is half of the Bragg angle corresponding to the (200) plane, and a factor of 57.3 was used to convert θ to radians. FWHM and peak position for (200) were determined from the diffractograms using Gaussian function peak fitting between 2θ of 18 and 29° .

- **2.7.** Nuclear Magnetic Resonance (NMR) Characterization of Cell Wall Polymers. Solubilized whole-cell walls of N and IN were analyzed by $^{1}\text{H}-^{13}\text{C}$ heteronuclear single quantum coherence (HSQC) 2D-NMR spectroscopy (Bruker Avance III 500 MHz instrument). Extractive-free biomass (200 mg) was milled into fine powder using a planetary ball mill (model: MPQ4X-V0.4L) using a ZrO₂ 50 mL jar and 3 and 6 mm Ø balls at 1000 rpm for 3 h. ²⁹ The fine powder (50 mg) was transferred to a 5 mm NMR tube, and dimethyl sulfoxide (DMSO)- d_6 /pyridine- d_5 (4:1, 0.7mL) was added and then sonicated for 30 min to form a gel. The spectra were collected at 30 °C with a Prodigy broadband cryo-probe, data were processed using Topspin 3.62 software, and the structures were colorcoded using three-dimensional (3D) paint.
- **2.8. Statistical Analysis.** To evaluate the compositional variation among four samples, analysis of variance (ANOVA) was performed at a 95% confidence level. Unless stated, RG1 and RG2 are statistically compared with D1 and D2, respectively.

3. RESULTS AND DISCUSSION

The Della and RG sorghum stalk N and IN samples (depicted in Figure 1a) were systematically characterized to observe differences between varieties and tissue types.

3.1. Lignin and Structural Carbohydrate Analysis. The KL and ASL total lignin (TL) content analyses of the two varieties at different N and IN are shown in Figure 1b-d. The KL was found to be 15.5-21.6, 9.4-16.3, 18.4-20.5, and 15.9-20.5% of the biomass, respectively, for D1, RG1, D2, and RG2 (Figure 1b). The KL results for sorghum N and IN are consistent with those in the literature.^{30,31} For D1, the KL at N1 and N2 was higher than the corresponding IN by 9.5 and 9.7%, respectively. However, KL at N3 was found to be less than its corresponding IN by 21.7%. Meanwhile, the variation of KL between N4 and IN4 within D1 stalks was not significant. The KL content of N was 16.1-42.5% higher than IN in RG1. However, the KL content of N and IN was similar for D2, except at N2, 6.8% less than IN2. On the other hand, IN2-IN4 of RG2 contained 10.0-13.6% higher KL than Ns. while IN1 had 6.5% less than N1. The overall KL content of RG2 was considerably reduced; particularly notable reductions along stalks at N3 and N4 (18 and 12.4%, respectively) were exhibited. RG1 displayed a significant reduction of KL: 16.5-44.3% at IN and 2.0-25.6% at Ns, as shown in Figure 1e. Between Della, the KL of D1 was found reduced (1.4-20.2%), except at N1, which could be related to seasonal changes. Sattler et al. 15 studied the KL of EMS-induced sorghum mutant lines and found variations for one of the cultivars.

The ASL content (Figure 1c) constituted a small fraction of the biomass: 2.0–3.4, 2.9–4.2, 2.4–3.0, and 2.1–3.1% for D1, RG1, D2, and RG2, respectively. The Ns had 14.6–37.0, 7.0–27.2, 13.8–20.4, and 19.8–33.6% higher ASL than IN for D1, RG1, D2, and RG2, respectively. Among the stalks, the highest ASL was found in RG1, increased by 18.4–57.3% compared to its counterpart D1 (Figure 1e). Contrarily, ASL in RG2 was 4.7–18.3% lower than D2 at all IN, whereas discrepancies were observed at N2 and N3 (Figure 1e).

The TL contents (Figure 1d) were 17.3-24.2, 12.7-20.5, 22.0-23.4, and 19.2-22.6% of the biomass, respectively, for D1, RG1, D2, and RG2, consistent with reported values.³² The TL content variations between IN and N of D2 were not significant, but the IN of D1 had less lignin (7.7–12%) than N, except at IN3. The TL content of RG1-IN was significantly lower (14.7-38.2%) than the corresponding N. On the other hand, RG2-IN has 5.6-9.7% more TL than its nodes, except at IN1. The TL of RG1 was significantly reduced at the IN by 5.6-34.6%. Other than RG1-N1, which was reduced by 20.7%, the N of D1 and RG1 contained similar lignin contents. The TL content of RG2 showed 6.4, 6.0, 14.3, and 15.1% reductions, respectively, at IN1, IN3, N3, and N4. Interestingly, the TL distribution of RG1 showed a major shift toward the N, where greater amounts of lignin are stored. Between the Della, the TL of D1 was reduced by 3.2-21.6%, except at N1, which could be related to seasonal and climatic changes.^{33,34} Across the mutants, the TL of RG1 was significantly reduced by 2.4-41%, except at N4. The result reveals that the combined effect of mutations and seasonal changes impaired the lignin content of RG1 more than RG2. Moreover, the finding on prominent TL reduction (Figure 1d) of RG1-IN suggests that the mutant is markedly impacted by the mutagenesis and environmental changes, consequently making it more susceptible to lignin reduction than the N. The limited

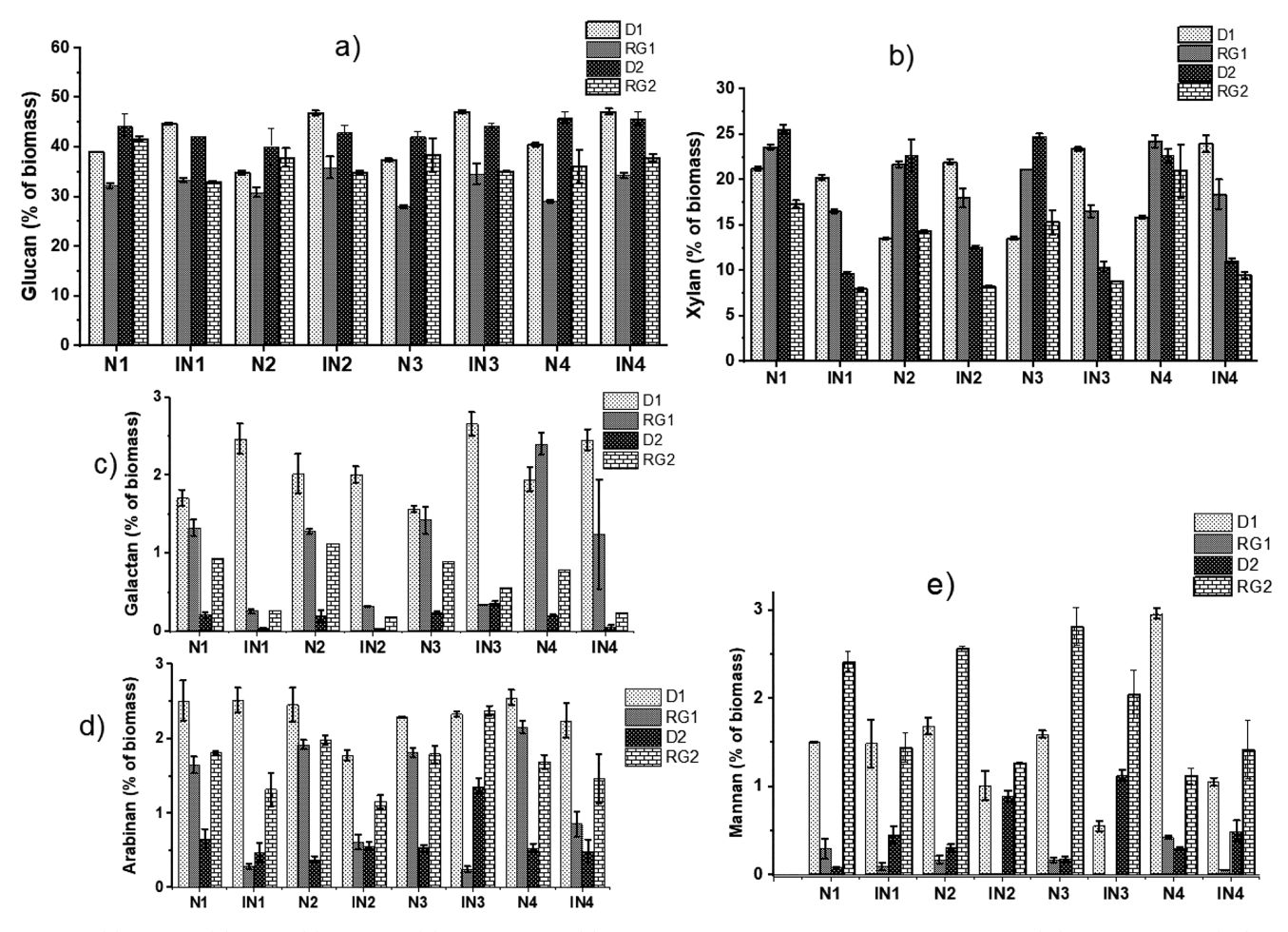


Figure 2. (a) Glucan, (b) xylan, (c) galactan, (d) arabinan, and (e) mannan contents of the sorghum stalk at nodes (N) and internodes (IN) for D1, RG1, D2, and RG2.

lignin content variation at different morphologies between D2 and RG2 suggests that RG2 was not as equally impacted as RG1. The lignin content variation between D1 and D2 also demonstrated the impact of growing seasons on lignin biosynthesis. Previous studies³⁵ showed that nodes are stronger, stiffer, and more rigid than internodes; hence, the greater lignin content at the nodes in RG1 could be related to natures' architectural design to avoid structural buckling of the cell wall of the mutant.⁸ Moreover, lignin is cross-linked with carbohydrates by covalent bonding to form LCC³⁶ and may play a role in maintaining the stiffness and mechanical recalcitrance of the cell wall. Thus, the stiffness of the RG1 stalk could be influenced by significant lignin reduction; subsequently, its lodging behavior could be likely impacted.¹⁴

The architecture and biological function of N are different from those of IN and are under genetic control.³⁷ Structural carbohydrate analyses at both IN and N for the mutants were compared with their respective Della; the results are shown in Figure 2. It was found in all varieties that glucan (cellulose) and xylan were the dominant polysaccharides and associated with the secondary cell wall of sorghum.³⁸ The glucan compositions were about 34–47, 28–38, 37–47, and 32–42% of the biomass and xylan compositions were about 13–25, 16–25, 11–26, and 8–26% of the biomass, respectively, for D1, RG1, 2, and RG2. Minor amounts (<3%) of galactan, mannan, and arabinan were also detected (Figure 2c–e). Along the stalks, N and IN of D2 had similar glucan contents

(about 43.6%). However, the glucan content between N and IN showed a significant variation in D1, RG1, and RG2 stalks. The N of RG2 had a higher average glucan content (38.5%) than IN (35.2%). Contrarily, the IN of D1 and RG1 had higher average glucan contents than their respective N: D1-IN (46.5%), D1-N (38.0%), RG1-IN (35%), and RG1-N (30%). This could be related to growth adaptation for more lignin repression at the IN.³⁹ The findings on sorghum stalk composition are consistent with those in the literature.^{30,40}

The glucan content of the Della variety was found to be significantly higher than its derivative mutants. In all N and IN analyzed, the glucan (Figure 2a) of RG2 was less than D2, giving a significant reduction of 17-22% for RG2-IN and 6-21% for RG2-N. Similarly, RG1 had less glucan content than the control D1: a reduction of 23-27% at IN and 11-28% at N was detected. Studies have shown a positive correlation between cellulose (glucan) deficiency and dwarfism in sorghum upon mutation.⁴¹ Among Della stalks, an increase in the glucan content of 3-9% at D1-IN and a decrease of 11-13% at D1-N were detected. RG-IN has a similar glucan content, whereas a significant reduction (18-27%) at RG1-N was recorded. The glucan composition of sorghum stem tissues is influenced by environmental conditions and photoperiod sensitivity and varies among varieties and different stem tissues.30

Xylan content analysis (Figure 2b) highlights that, within each RG1, D2, and RG2 stalk, the N contained significantly

more xylan than IN. The average xylan contents were RG1-IN (17.4%), RG1-N (22.7%), D2-IN (11.7%), D2-N (23.9%), RG2-IN (8.6%), and RG2-N (17.0%). However, D1-IN has more average xylan (22.4%) than N (17.2%). The results agree with those in the literature. Across the varieties, 14–35 and 7–38% reductions, respectively, at RG2-IN and RG2-N were recorded. Meanwhile, xylan reduction of 18–29% at RG1-IN and an increase of 11–60% at RG1-N were observed. Xylan variations at different sorghum stalk components have been reported. Variation in galactan, arabinan, and mannan (Figure 2c–e) contents among varieties has also been detected.

3.2. FTIR Spectral Analysis of Biomass. FTIR spectroscopy has been used to investigate the functional groups of cellulose, hemicelluloses, and lignin of the IN for the sorghum varieties (Figure 3). Spectral assignments are given in Table

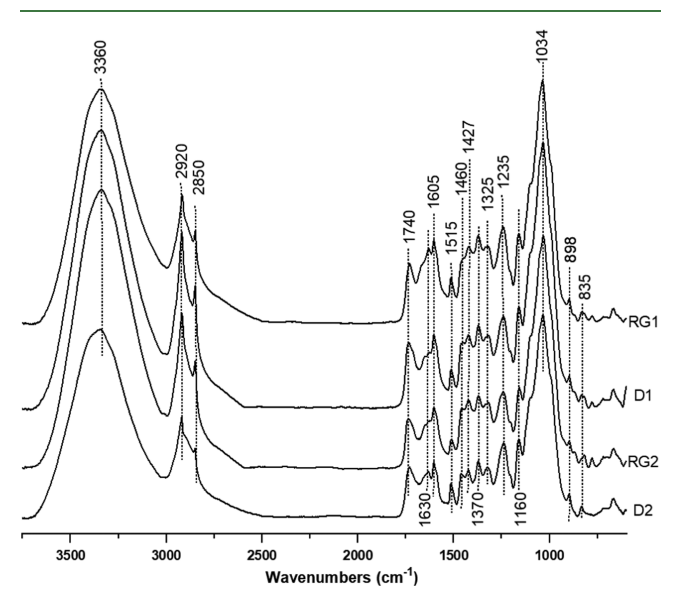


Figure 3. FTIR spectra of sorghum stalks for D2, RG2, D1, and RG1 at the internodes.

S1. Analysis of the spectra of biomass samples shows that the fingerprint region of the IN (1800-900 cm⁻¹) contains important information pertaining to the functional groups of carbohydrates and lignin (Figure 3). The spectra of Della and RG varieties exhibited similar absorption bands. The strong absorbance band at 1034 cm⁻¹ was attributed to glycosidic bonds (C-O-C) in carbohydrates.⁴⁴ Other polysaccharide bands include 1375 cm⁻¹, attributed to C–H bending in cellulose and hemicellulose,⁴⁵ and 898 cm⁻¹, attributed to the C-H deformation in cellulose. For lignin, the band at 1165 cm⁻¹ assigned to C=O stretching from conjugated ketone and ester groups, 46 1235 cm⁻¹ from C=O, C-O, and C-C bendings in guaiacyl (G) units,⁴⁷ 1325 cm⁻¹ due to syringyl units (S) ring breathing, and 1515 cm⁻¹ attributed to the C= C stretch of the aromatic skeleton were all detected. The broad band centered at 1740 cm⁻¹ was assigned to C=O stretching of esters (acetyl groups), carboxylic acids, and unconjugated ketones in xylan and lignin. The conjugated C=O (1630 cm⁻¹) suggests the presence of noncanonical p-hydroxycinnamates (p-coumaric acid (pCA) and ferulic acid (FA)) in the stalks. 48 The band at 1460 cm⁻¹ was assigned to asymmetric bending of CH₂ in cellulose and CH₃ in methoxy (CH₃-O) groups. 49 The typical HGS bands at 1160 and 835 cm⁻¹ (C-H

out-of-plane in syringyl and *p*-hydroxyphenyl units) confirms an HGS-type lignin. The band at 1160 cm⁻¹ corresponds to asymmetric C–O stretching of an ester and is most likely due to acetyl groups.¹⁹

Features of cellulose (TCI and LOI) were determined from FTIR spectroscopy and are summarized in Table 1. The TCI

Table 1. Total Crystallinity Index (TCI), Lateral Order Index (LOI), and S/G Ratio Determined on Sorghum Biomass by FTIR Spectral Analysis

variety	TCI	LOI	S/G
D2-IN	57.9 ± 2.0	2.14 ± 0.11	0.49 ± 0.01
RG2-IN	51.7 ± 2.1	2.38 ± 0.05	0.66 ± 0.01
D1-IN	49.4 ± 1.1	2.18 ± 0.04	0.63 ± 0.01
RG1-IN	64.1 ± 1.9	3.05 ± 0.14	0.77 ± 0.03
D2-N	68.8 ± 1.9	2.00 ± 0.08	0.54 ± 0.02
RG2-N	49.0 ± 5.8	2.38 ± 0.12	0.62 ± 0.03
D1-N	49.5 ± 2.2	2.66 ± 0.09	0.56 ± 0.01
RG1-N	62.0 ± 3.2	3.38 ± 0.21	0.62 ± 0.01

 (I_{1370}/I_{2920}) values were 0.49, 0.62-0.71, 0.58-0.69, and 0.49-0.52, respectively, for D1, RG1, D2, and RG2. The results are consistent with TCI values determined for Sorghum bicolor. 50 The average TCI values for D2 were higher than for average RG2, which supports the higher glucan/cellulose content in the structural carbohydrate analysis and crystallinity index by XRD (discussed later). Nevertheless, the TCI for RG1 was higher than that of D1. This suggests that D1 has more amorphous cellulose than RG1, while the XRD (discussed later) shows comparable crystallinity between the two varieties. As shown in Table 1, the LOI values for the Della variety were lower than their corresponding RG variety, which might arise from the cellulose structural difference in the varieties. Besides, the intensity at 1370 cm⁻¹ may be influenced by the neighboring lignin IR band at 1325 cm⁻¹. The LOI increased with the crystallinity of cellulose I.51 FTIR spectra of the biomass also provided information on lignin composition (e.g., S/G ratio). The S/G ratios for D2, RG2, D1, and RG1 were 0.49-0.54, 0.62-0.66, 0.56-0.63, and 0.62-0.84, respectively. The S/G ratio (Table 1) of RG was significantly higher than Della. These S/G values are comparable to those of grass lignin. ⁵² FTIR spectroscopy was employed to categorize lignin of different biomass origins ⁴⁷ and detect S/ G ratio variations of different biomass varieties.⁵⁰

3.3. Analytical Py-GCMS Analysis. Analytical Py-GCMS analysis was used to determine sorghum stalk compositional differences and the H/G/S ratio of lignin (Figure 4). The pyrograms showed the presence of carbohydrate and lignin thermal degradation products at IN (Table S2) and N (Table S3). The pyrograms of RG1 at both IN and N were different (Figures S1 and S2) than those of D2, RG2, and D1. Despite the presence of common pyrolysate products and general pyrolysis trends, the result revealed that the pyrolysis behavior of the varieties was different, resulting in distinct products likely due to differences in their compositional and structural variation. Most of these pyrolysis products have been detected in previous Py-GCMS studies of biomass in different abundances. ⁵⁰

The S/G ratio is a crucial indicator of the degree and nature of cross-linking between lignin subunits. The G-rich lignin is more cross-linked than the S lignin.⁵³ The S/G ratios of D2, RG2, D1, and RG1 calculated from Py-GCMS chromatograms

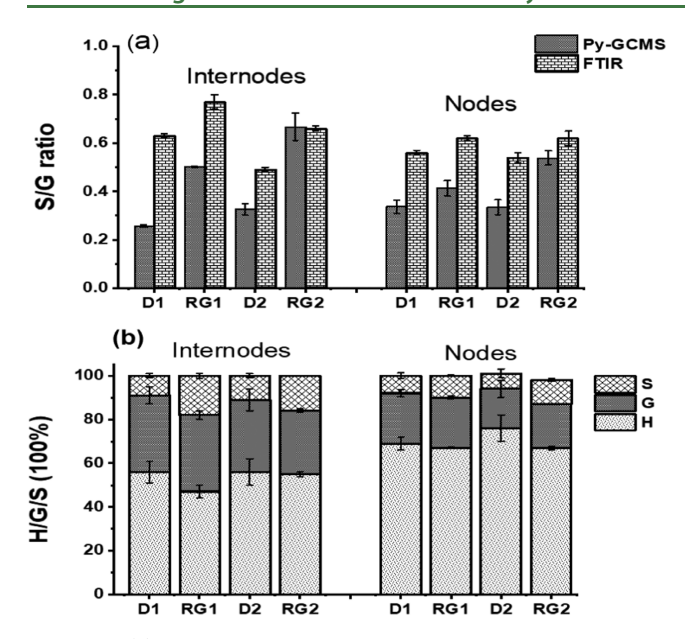


Figure 4. (a) S/G ratio comparison determined by Py-GCMS and FTIR at internodes (IN) and nodes (N) and (b) the distribution of *p*-hydroxyphenyl (H), guaiacyl (G), and syringyl (S) lignin from Py-GCMS (H/G/S in %) for D1, RG1, D2, and RG2, varieties at IN and N.

and FTIR spectra are given in Figure 4a. The Py-GCMS result shows that the S/G ratios of mutants were significantly increased from their corresponding Della. The S/G ratios of D2 were about 0.32 (IN) and 0.33 (N) and those for D1 were IN (0.25) and N (0.33), which are comparable to coconut shell powder (S/G = 0.27) and oats husks (S/G = 0.36).⁵⁴ An S/G ratio increase of more than 2-fold at IN and 61% at N was recorded for RG2. However, in RG1, S/G increases of about 96% at IN and 23% at N were observed (Figure 4a). An increase in the S/G ratio for RG1 stems has been reported by Petti et al. 16 The result shows that the G-type lignin in RG2 and RG1 was reduced, while the S lignin had increased, resulting in a relatively higher S/G ratio. In Py-GCMS-based determination of the S/G ratio, the G-type lignin may be overestimated, as ferulates are also decarboxylated to 4vinylguaiacol upon pyrolysis, 55 which leads to an underestimated S/G ratio. It is known that ferulates have been detected in 2D-NMR (discussed later) in the stalks. Some studies^{56,57} have suggested ignoring 4-vinylguaiacol and 4vinylsyringol in wheat/grasses for determining the S/G ratio, considering that the two lignin products are released primarily from noncanonical lignin monomers/cinnamates. However, ignoring the two lignin products leads to a significantly lower S/G ratio than reported for our samples. An increase in S/G may weaken the three-dimensional lignin structure and thus decrease the lignin's glass-transition temperature (and modulus)⁵⁸ and contribute to a reduced bending strength of the stalk, ultimately influencing resistance to lodging.⁵⁹ Considering the total lignin content analysis, RG2 mainly showed lignin compositional change, whereas RG1 showed both lignin content reduction as well as its composition. The results are consistent with those of previous studies.³² The FTIR spectral S/G ratio analysis followed the same trend as Py-GCMS: a significant increase by 10-22 and 16-32% for RG1 and RG2, respectively. Except at RG2-IN, the S/G ratio determined by FTIR was higher than by Py-GCMS, as shown in Figure 4a at IN and N. Using the same method, corn stover

(S/G = 0.48) and switchgrass lignin (S/G = 0.43) were reported.⁵² The detection of a relatively higher S/G ratio by FTIR could be due to the complex nature of the cell wall and the band interference/overlap from carbohydrates.⁶⁰

The relative H/G/S peak area distribution from the Py-GCMS (Figure 4b) confirms the H/G/S type of lignin in sorghum. The presence of p-coumarates (confirmed by FTIR and 2D-NMR), which decarboxylate during pyrolysis, is primarily responsible for the detection of large amounts of 4vinylphenol during pyrolysis. 55 Thus, 4-vinylphenol was ignored in H/G/S estimation. For the IN, the H/G/S ratios were found to be 56/33/11, 40/36/24, 56/35/9, and 47/35/ 18, respectively, for D2, RG2, D1, and RG1. The H/G/S ratios for nodes were 76/18/7, 69/20/11, 69/23/8, and 67/23/10 for D2, RG2, D1, and RG1, respectively. H/G/S Ratios have been reported for different grass families: switchgrass (26/42/ 32),⁶¹ miscanthus (4/44/54),⁶² maize (9/58/33),⁵⁴ and wheat (6/58/36). As reactive sites for interunit linkages (H > G > S),53 a higher content of S lignin in RGs may lead to a lower number of carbon-carbon and more β -O-4 ether linkages and lower lignin's glass-transition temperature and modulus.⁶

3.4. TGA Analysis. Thermal decomposition behavior of the four sorghum stalks at the IN was investigated by TGA as a rapid method to distinguish between varieties (Figure 5). The

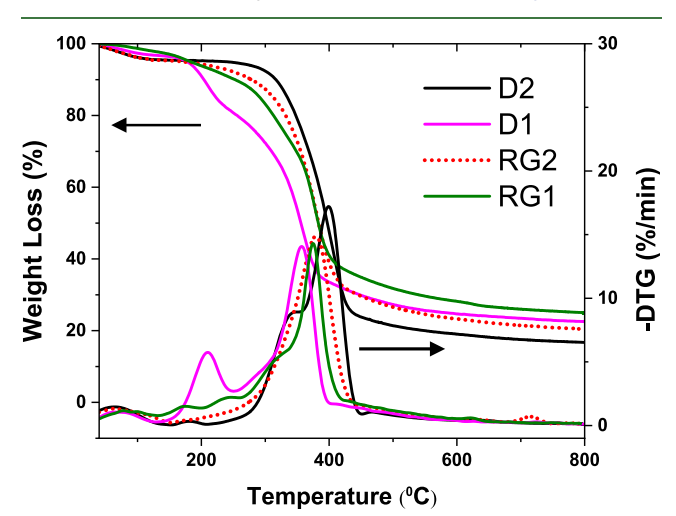


Figure 5. TGA thermograms of D2, D1, RG2, and RG1 sorghum biomass at IN (y-axis on the right is the differential thermogravimetric (DTG) of stalks).

thermogram shows different stages of weight losses in relation to the thermal stability of hemicellulose, cellulose, and lignin. The first stage (40–120 °C) is associated with water loss. The second stage (180–340 °C) is attributed to degradation of mainly hemicellulose (xylan) and shows distinct shoulders for D2 (340 °C) and RG1 (310 °C) and a peak for D1 (210 °C) varieties. However, no shoulder/peak was detected in RG2. These variations are likely attributed to differences in the hemicellulose structure. The third stage (340–400 °C) corresponds to cellulose decomposition. Lignin decomposes over a wide temperature range due to dissimilar thermal stabilities of its functional groups. It is believed that lignin pyrolysis starts at the third stage and continues to the final stage of degradation (long tail above 400 °C). These TGA findings are in agreement with sorghum² and corn stalk studies.

Previous studies have shown that the thermogravimetric (TG) curve varies with cellulose, hemicellulose, and lignin contents⁶⁸ and biomass type.⁷¹ The residue char/ash left at 800 °C for D1, RG1, D2, and RG2 were, respectively, 22.5, 24.9, 16.6, and 19.9% (Table 2). The onset temperature (T_{onset}) for the major weight loss transition varied for the different sorghum varieties (Table 2).

Table 2. Residual Mass at 800° C and Major Onset Temperatures (T_{onset}) of D2, RG2, D1, and RG1 Stalks

sorghum	residual mass at 800 °C (%)	$T_{ m onset}$ (°C)
D1	22.5 ± 0.4	357 ± 1
RG1	24.9 ± 0.1	377 ± 1
D2	16.6 ± 0.2	403 ± 1
RG2	19.9 ± 0.5	385 ± 5

3.5. XRD Analysis. In plant cell walls, glucan chains of cellulose form long threadlike microfibrils, which may be partly crystalline. The crystallinity of the microfibrils in the sorghum samples was evaluated by XRD (Figure 6a), and its

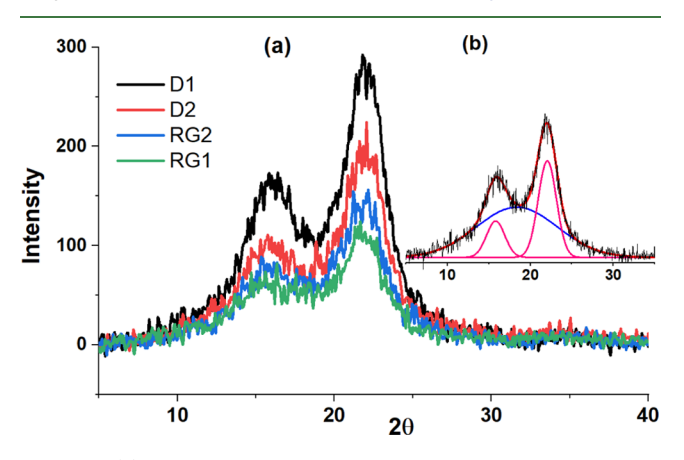


Figure 6. (a) X-ray diffractogram of D1, D2, RG2, and RG1 sorghum biomass at IN and (b) deconvolution of the peaks using peak fitting of D1.

peak fitting is shown in Figure 6b. The XRD analysis confirms the two-state structures: a broad amorphous structure indicated at 2θ of about 18.5° (mainly from hemicellulose, lignin, and amorphous cellulose) and distinct crystalline cellulose peaks at 2θ of 15.5 [Miller indices of $(1\bar{1}0)$ and (110) overlapped], and 21.9° assigned to (200) lattice indices. The crystallinity indexes (CI_d and CI_h) for IN were calculated from the XRD data, and the results are given in Table 3. For D2, the CI_d and CI_h were 12 and 6% higher than RG2, while the D1 and RG1 had similar crystallinity indexes for both methods. The CI_d values are comparable to those in the literature. Petti et al. reported no variation between

Table 3. Crystallinity Index of D1, RG1, D2, and RG2 at IN Based on Peak Deconvolution (CI_d) , Peak Height (CI_h) Methods, and Average Grain Size (L) of Cellulose at (200)

sorghum	CI _d (%)	CI _h (%)	L (nm)
D1	32.0 ± 1.3	58.2 ± 1.9	3.3 ± 0.0
RG1	31.8 ± 0.9	58.1 ± 1.0	3.2 ± 0.1
D2	38.0 ± 1.0	63.3 ± 0.2	3.0 ± 0.1
RG2	33.5 ± 0.6	59.4 ± 0.6	3.1 ± 0.0

sorghum cultivars.¹⁶ The cellulose microcrystalline grain size in the (200) plane was comparable for all samples at about 3 nm (Table 3). The shape and crystallinity of microfibrils may impact the biomechanical properties of the stalks.

3.6. Nuclear Magnetic Resonance (NMR) Spectroscopy of Cell Walls. Dissolved-gelatinized cell walls of N and IN sections from D2, RG2, D1, and RG1 sorghum stalks were analyzed by 2D ¹³C-¹H HSQC NMR spectroscopy to elucidate lignin interunit linkages and structures. Spectral assignments were based on the works of Kim and Ralph, ^{29,75} Yuan et al.,³⁶ Balakshin et al.,⁷⁶ and Komatsu and Kikuchi.⁷⁷ The types of interunit linkages in lignin monomers are found in the side-chain region ($\delta C/\delta H$ 50–90/2.5–5.0 ppm) of the 2D-HSQC spectra cross-peaks. The distribution of lignin linkages in the side-chain regions of IN and N sections of D1, RG1, D2, and RG2 is compared and shown in Figure 7. Polysaccharide-associated signals are also observed in this spectra region. The characteristic signals at $\delta C/\delta H$ 55.6/3.73 ppm and $\delta C/\delta H$ 60.95/3.57 ppm corresponding, respectively, to methoxy groups and $C\gamma/H\gamma$ units in G-type β -O-4 linkages (Ay) were observed in all samples.³⁶ For all varieties and N and IN sections, the β -O-4 aryl ether linkage was the major lignin linkage. An important feature observed in the HSQC spectra from the stalks was the occurrence of strong signals from γ -acylated β -O-4 alkyl aryl ethers. The occurrence of intense signals at around $\delta C/\delta H$ 63.04/3.94 ppm, assigned to the C_{ν}/H_{ν} correlations of γ -acylated β -O-4 $(A\gamma')$ substructures, revealed that a significant part of the lignin from stalks was acylated at the γ -position of the lignin side chain. Other types of lignin linkages such as phenylcoumaran $(\beta-5)$ units, resinol $(\beta-\beta)$ units, and dibenzodioxocin (5-5) $4-O-\beta$) were not detected, consistent with reported results for corn stalks.²⁹ Complete cross-peak assignments and linkage (Table S4) and all possible lignin linkage structures (Figure S4) are provided in the Supporting Information.

The 2D-HSQC spectra of D1 (Figure 7a,e) show signals with relatively similar profiles between the N and IN, except for the detection of $Xylp_{(3)}$ at the N, whereas $Xylp_{(2)}$ was observed at IN. Among the lignin interunit linkages, signals for $A\gamma$, $A\gamma'$, and methoxy were detected in both N and IN. The detection of cinnamyl acetate substructures Cy/Hy (66.63/ 4.48 ppm)⁷⁸ is a distinct feature of D1 compared to the other three sorghum samples. Other xylan- and arabinan-related substructures were also observed, as shown in Figure 7a,e. On the other hand, the spectra of RG1 stalks (Figure 7b,f) were also shown to be different from those of D1 in that 2-O-acetyl- β -D-xylopyranosyl structural units were only observed in RG1. Like RG2 and D1, (1,3)- α -L-arabinofuranosyl, (1,2)- α -Larabinofuranosyl, and C_4/H_4 in $(1 \rightarrow 4)-\beta$ -D-xylopyranosyl units with nonreducing ends were distinct structural features of RG1 but not D2. The cross-peaks for $(1,2)-\alpha$ -L-arabinofuranosyl units in RG1 were shown to overlap with other unassigned cross-signals. On the other hand, structural features between N and IN in RG1 were similar. Signals attributed to C_2/H_2 in $(1 \rightarrow 4)$ - β -D-xylopyranosyl, C_3/H_3 in $(1 \rightarrow 4)$ - β -Dxylopyranosyl, C_4/H_4 in $(1 \rightarrow 4)$ - β -D-xylopyranosyl, and C_5/H_4 H_5 in $(1 \rightarrow 4)$ - β -D-xylopyranosyl units together with lignin linkages of A γ and A γ' were detected. However, signals for $C\alpha/H\alpha$ in β -O-4 substructures were not observed in D1 and

For the D2, the HSQC spectra for the IN and N (Figure 7c,g) were similar, except that a weaker signal at 61.71/4.16 ppm corresponding to the $C\gamma/H\gamma$ cinnamyl alcohol end group

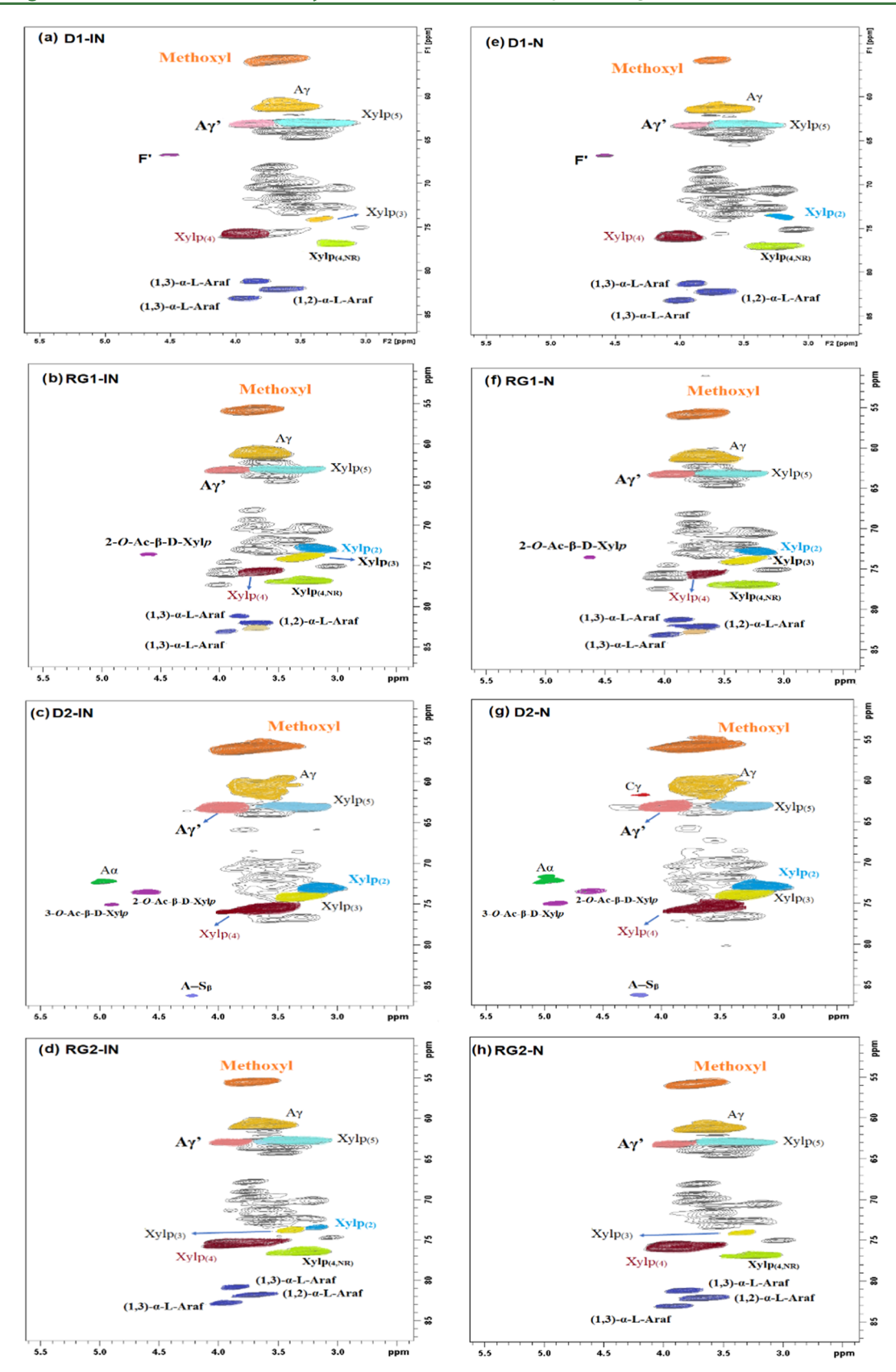


Figure 7. 2D HSQC ¹H-¹³C correlation NMR spectra of the aliphatic region of the sorghum stalk cell wall: (a) D1-IN, (b) RG1-IN, (c) D2-IN, (d) RG2-IN, (e) D1-N, (f) RG1-N, (g) D2-N, and (h) RG2-N. Gray colors in the contours are either unassigned due to a lack of reliable information or unresolved.

was detected in the N sample, which shows some structural variation between tissue types. Strong signals were observed

for methoxy and A γ . Furthermore, C α /H α correlations in β – O–4 (A α) substructures were observed at δ C/ δ H 72.23/4.96

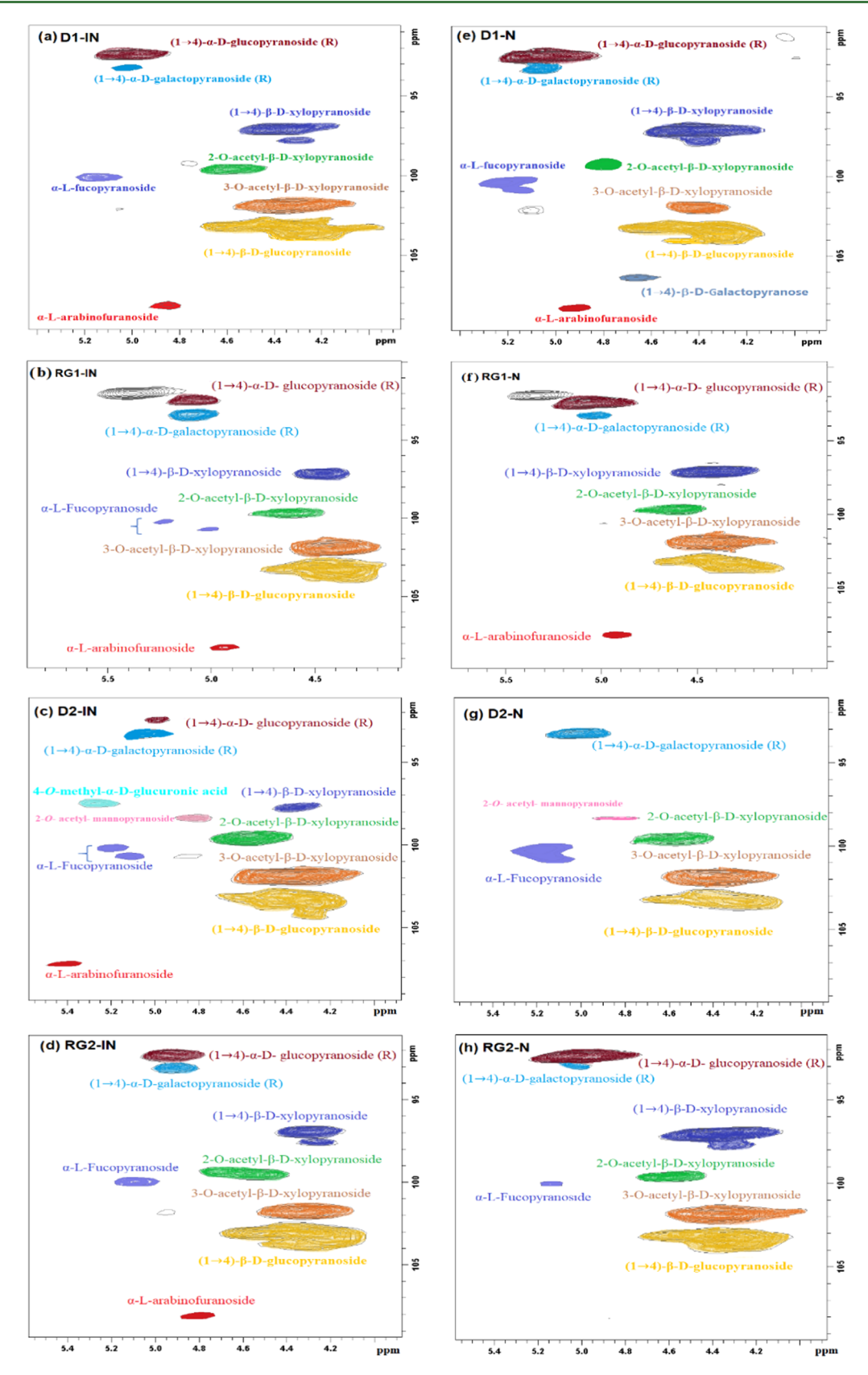


Figure 8. Polysaccharide anomeric regions from 2D HSQC 1H $_{-}^{13}$ C correlation NMR spectra for the gel states of four sorghum whole-cell wall samples at the nodes (N) and internodes (IN) in DMSO- d_6 /pyridine- d_5 (4:1) solvent: (a) D1-IN, (b) RG1-IN, (c) D2-IN, (d) RG2-IN, (e) D1-N, (f) RG1-N, (g) D2-N, and (h) RG2-N. R refers to the reducing end, and gray cross-links in RG1 are unassigned carbohydrates.

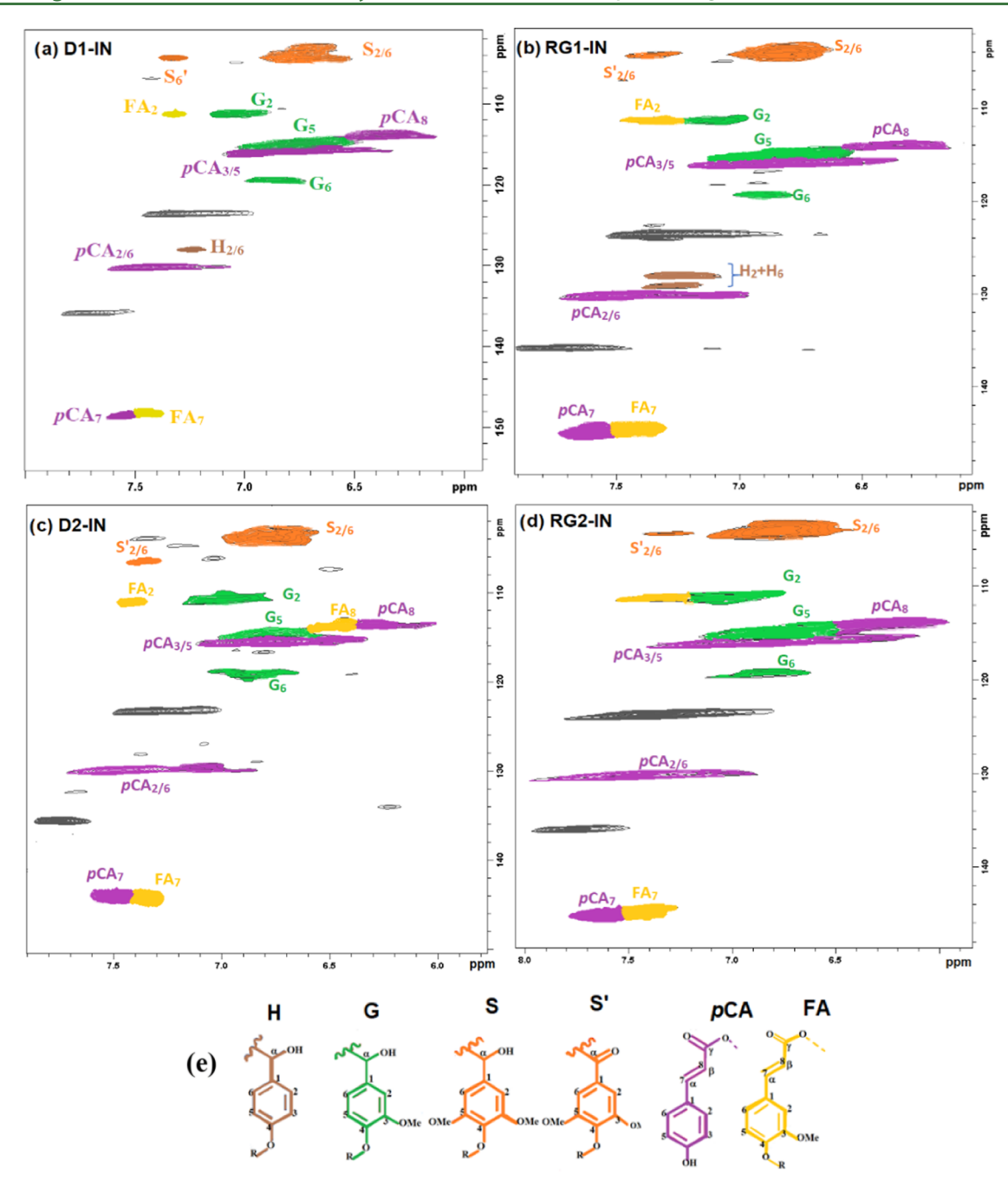


Figure 9. 2D HSQC 1 H- 13 C correlation NMR spectra of sorghum whole-cell wall gels in DMSO- d_{6} /pyridine- d_{5} (4:1) solvent in the aromatic region at internodes (IN) (a) D1-IN, (b) RG1-IN, (c) D2-IN, and (d) RG2-IN and (e) lignin structures: p-hydroxyphenyl units (H), guaiacyl units (G), syringyl units (S), oxidized syringyl units at C α (S'), p-coumarate (pCA), and ferulate (FA). The signals in black/gray correspond to pyridine- d_{5} .

ppm. In addition, the correlation at $\delta C/\delta H$ 86.21/4.20 ppm was shown to correspond to S-type β -O-4 (A-S $_{\beta}$) substructures. ⁸⁰

The hemicellulose (xylan) was identified in the D2 sorghum stalks by the presence of acetyl groups at $\delta C/\delta H$ 73.51/4.61 ppm, which corresponds to C_2/H_2 in 2-O-acetyl- β -D-xylopyranosyl units and $\delta C/\delta H$ 75.00/4.91 ppm for C_3/H_3 in 3-O-acetyl- β -D-xylopyranosyl units. These two signals for the acetylated structures were not detected in both the N and IN of RG2 and D1, while only the 2-O-acetyl- β -D-xylopyranosyl structure was observed in RG1. The spectra also show $\delta C/\delta H$ signals at 72.83/3.16 ppm for C_2/H_2 in (1

→ 4)- β -D-xylopyranosyl, 74.04/3.35 ppm for C_3/H_3 in (1 → 4)- β -D-xylopyranosyl, 75.51/3.63 ppm for C_4/H_4 in (1 → 4)- β -D-xylopyranosyl, and 63.12/3.27 ppm for C_5/H_5 in (1 → 4)- β -D-xylopyranosyl.

In RG2, the N showed signals for the C_2/H_2 in $(1 \to 4)$ - β -D-xylopyranosyl units but were absent in the IN. In comparison with the D2, the RG2 was noticeably different. In terms of linkages, $A\alpha$ substructures were not observed in RG2, whereas signals from $A\gamma$, $A\gamma'$, and methoxy were detected (Figure 7d,h). Other distinct structures and signals for the RG2 samples in the side-chain region include C_2/H_2 for (1,3)- α -L-arabinofuranosyl at $\delta C/\delta H$ 80.81/3.86 ppm and 82.69/3.96

ppm and (1,2)- α -L-arabinofuranosyl units at $\delta C/\delta H$ 81.73/3.69 ppm. ⁸¹ These results support relatively higher arabinan contents from carbohydrate analysis. Moreover, the C₄/H₄ in the (1 \rightarrow 4)- β -D-xylopyranosyl unit with a nonreducing end at $\delta C/\delta H$ 76.82/3.22 ppm was also observed. ²⁹ Other carbohydrate signals attributed to C₂/H₂ in (1 \rightarrow 4)- β -D-xylopyranoside, C₃/H₃ in (1 \rightarrow 4)- β -D-xylopyranoside, C₄/H₄ in (1 \rightarrow 4)- β -D-xylopyranoside units were also detected. ⁸² All of these structural variations may contribute to property differences among the stalks of D1, RG1, D2, and RG2.

The main notable linkages detected were nonacylated β -O-4 and naturally γ -acylated β -O-4 (Figure S4). Thus, for the purpose of identifying their relative abundance and providing explicit information of structural difference among the samples, quantitative analysis as a percentage of these chains was performed. The degree of γ -acylation of the lignin side chains was estimated from the C_v/H_v correlation signals in β -O-4 and γ -acylated β -O-4 alkyl aryl ethers. Accordingly, the percentages of acylation $(A\gamma/A\gamma')$ were 79.0/21.0, 85.0/ 15.0, 83.0/17.0, and 88.0/12.0 for IN of D1, RG1, D2, and RG2, respectively. The result shows significant variation in the degree of acylation between RG and Della varieties, revealing that more naturally γ -acylated β -O-4 linkages at IN of the Della variety were identified than RG in both growing seasons, which shows the nature of lignin variation. Naturally occurring acylated lignin has been identified in different plants. 83 For the N, $A\gamma/A\gamma'$ values of D1 (90.0/10.0), RG1(88.0/12), D2 (82.0/18.0), and RG2 (88.0/12.0) were detected.

The polysaccharide anomeric region in the HSQC spectra (90–110/4.0–6.0 ppm) of the IN and N (Figure 8) provides key information on the composition of the various polysaccharides and their substituents.^{29,36,81} Clearly resolved polysaccharide anomeric correlations were detected in all cell wall samples (Table S4).

The spectra of D1 in the anomeric region (Figure 8a,e) show that strong signals attributed to $(1 \rightarrow 4)$ - β -D-glucopyranosyl units (103.15/4.34 ppm) were detected at both IN and N. Besides, $(1 \rightarrow 4)$ - α -D-glucopyranosyl (R), $(1 \rightarrow 4)$ - β -D-xylopyranosyl, 3-O-acetylated- β -D-xylopyranosyl, 2-O-acetylated- β -D-xylopyranosyl, and α -L-fucopyranosyl units were detected in both IN and N. In contrast to IN of D2, RG2, and RG1, the $(1 \rightarrow 4)$ - α -D-galactopyranosyl (R) units were weaker in D1-IN. Unlike the N of D2, RG2, and RG1, D1-N had distinct cross-signals at 108.09/4.85 ppm and 106.3/4.60 ppm, respectively, from α -L-arabinofuranosyl and $(1 \rightarrow 4)$ - β -D-galactopyranosyl (not detected in D1-IN) units (Figure 8e). Moreover, a relatively weak signal of 3-O-acetylated- β -D-xylopyranosyl (101.86/4.34 ppm cross-peak) was detected in the D1-N sample.

The HSQC spectra of RG1 in the anomeric region (Figure 8b,f) showed a distinctive and prominent signal at 91.83/5.30 ppm, the unassigned carbohydrate that makes RG1 different from D2, D1, and RG2. Like D2, RG2, and D1, prominent signals attributed to $(1 \rightarrow 4)$ - α -D-glucopyranosyl, $(1 \rightarrow 4)$ - β -D-glucopyranosyl, 3-O-acetylated- β -D-xylopyranosyl, and 2-O-acetylated-xylopyranosyl units were detected in RG1. Comparison of the anomeric features of IN and N of RG1 (Figure 8b,f) indicated the same profile, except for slight differences—the weaker signal from nodes associated with $(1 \rightarrow 4)$ - α -D-galactopyranosyl units at 94.26/5.08 ppm.

The spectra of the D2 (Figure 8c,g) anomeric region (C1/H1) show prominent signals for $(1 \rightarrow 4)-\alpha$ -D-galactopyranosyl

units (reducing end, R) at 93.29/5.04 ppm, 2-O-acetylated- β -D-xylopyranosyl units at 99.32/4.63 ppm, 3-O-acetylated- β -D-xylopyranosyl units at 101.56/4.38 ppm, and (1 \rightarrow 4)- β -D-glucopyranosyl units at 103.01/4.30 ppm. A strong signal from α -L-fucopyranosyl units at 100.72/5.12 ppm was detected in N and IN samples. On the other hand, comparison of the spectra between the IN and N (Figure 8c,g) revealed different signals for the IN material. Particularly, (1 \rightarrow 4)- α -D-glucopyranosyl units (R) at 92.38/5.06 ppm, 4-O-methyl- α -D-glucuronic acid at 97.48/5.26 ppm, the (1 \rightarrow 4)- β -D-xylopyranosyl unit (R) at 97.10/4.40 ppm, and the α -L-arabinofuranosyl unit at 107.17/5.41 ppm were only detected at the IN. Similar findings were observed, by HSQC, on corn cell walls.

The anomeric positions (C_1/H_1) for RG2 samples for IN and N (Figure 8d,h) showed a similar spectrum, except for the α -L-arabinofuranosyl unit, which was only detected at the IN, and the $(1 \rightarrow 4)$ - α -D-galactopyranosyl unit (R) at 93.29/5.04 ppm and $(1 \rightarrow 4)$ - β -D-glucopyranosyl at about 103.01/4.30 ppm were not resolved well for the N. The signal strength of (1 \rightarrow 4)- β -D-glucopyranosyl at the N was higher than at the IN. Contrarily, α -L-fucopyranosyl units at the N were of low intensity. In comparison with D2, the signal strength of $(1 \rightarrow$ 4)- β -D-glucopyranosyl units of RG2 were strong. Moreover, unlike D2, signals of 4-O-methyl- α -D-glucuronic acid and 2-Oacetylated-mannopyranosyl units for RG2 were absent, revealing structural variations between the two. Unlike the N in the D2, $(1 \rightarrow 4)$ - β -D-xylopyranosyl units were detected at the N of RG2. Likewise, notable anomeric signals associated with $(1 \rightarrow 4)$ - α -D-glucopyranosyl, 3-O-acetylated- β -D-xylopyranosyl, and 2-O-acetylated-xylopyranosyl units were also detected.75

The aromatic regions ($\delta_{\rm C}/\delta_{\rm H}$ 100–150/6.0–8.0 ppm) of D1, RG1, D2, and RG2, samples in the 2D-HSQC spectra at the IN and N are given in Figures 9 and S3. This region contains correlations of guaiacyl (G), syringyl (S), and oxidized syringyl (S') units at ${\rm C}_\alpha$ =O and hydroxycinnamates (ferulate, FA, and p-coumaric acid, pCA) and limited p-hydroxyphenyl (H). Moreover, signals attributed to hydroxycinnamates were also detected in D1. The S units were detected in two forms: at correlations of $\delta_{\rm C}/\delta_{\rm H}$ 103.48/6.75 ppm and $\delta_{\rm C}/\delta_{\rm H}$ 104.12/7.43 ppm (${\rm C}_{2/6}/{\rm H}_{2/6}$), respectively, for S units and an oxidized S lignin (S') at ${\rm C}\alpha$ -ketone. The S' units were minor, showing that the possible oxidation of S units either during sample preparation or during lignification was limited.

The HSQC of D1 in the aromatic region for IN (Figure 9a) and N (Figure S3a) has similar spectra except for the relatively higher signal of the H lignin at 127.92/7.26 ppm and the detection of FA8 at the nodes. Correlation peak assignments are provided in Table S4. The signals from both guaiacyl $(G_2,$ G_5 , G_6) and syringyl $(S_{2/6})$ units were readily observed from the signals centered at 111.18/7.10, 115.05/6.86, 119.30/6.88, and 03.6/6.8 ppm in both IN and N. On the other hand, the stalks of RG1 consisted of a relatively strong signal at correlations of about 127.92/7.26 and 129.02/7.27 ppm from $C_{2/6}/H_{2/6}$ of H units at both the nodes (Figure S3b) and internodes (Figure 9b). Similar reports were found and have been published for Arabidopsis.⁸⁴ Like the control group (D1), G_2 , G_5 , G_6 , and $S_{2/6}$ were also observed in RG1. Significant amounts of p-coumarates in both control and mutant RG1 samples were observed at both N and IN. In addition, ferulate units were also detected for IN (Figure 9a,b) and N (Figure S3a,b) in both D1 and RG1 samples. Ferulate

and *p*-coumarate units were detected in wild and transgenic switchgrasses⁸⁰ and forage sorghum. ¹⁹ Unlike the N of D2, RG2, and D1, FA₈ was not detected at both the N and IN of RG1 stalks.

The HSQC spectra of the D2 whole-cell wall in the aromatic region (Figures 9c and S3) show that the weaker signal corresponding to the H_{2/6} aromatic correlation from H units at 127.92/7.26 ppm was detected only at the N. Besides H units, the other distinct features between the N and IN of D2 come from ferulate units. Ferulates are involved in acylating arabinoxylans, lignification, and cross-coupling lignin monomers with oligomers forming lignin-carbohydrate complexes (LCC).²⁹ Ferulate-related signals were observed at 110.91/ 7.07, 115.19/6.5, and 144.27/7.42 ppm, respectively, for C_2 / H₂, C₈/H₈, and C₇/H₇ of ferulic acid (FA). S As seen in the spectra, FA₃ in the N (Figure S3) overlapped with pCA_{3/5}, whereas in the IN, it overlapped with G₅ and pCA₈. Strong and well-resolved signals attributed to $C_{2,6}/H_{2,6}$ of S units at $\delta_{\rm C}/\delta_{\rm H}$ (103.48/6.75 ppm) were detected. Moreover, the aromatic region was relatively dominated by cross-signals associated with pCA at 115.46/6.78 ppm from $C_{3/5}/H_{3/5}$ residues, 129.84/7.48 ppm from $C_{2/6}/H_{2/6}$, 113.54/6.31 ppm from $C_8/$ H₈, and 144/7.5 ppm for C₇/H₇. Furthermore, G-ligninassociated contour signals were also detected at $\delta_C 6/\delta_H$ 110.07/6.98, 114.59/6.79, and 119.09/6.86 ppm, respectively, for C_2/H_2 , C_5/H_5 , and C_6/H_6 residues of G units.

The HSQC correlations of the aromatic region of RG2 revealed that FA_8 and $H_{2/6}$ were not detected at the IN. Yet, like D2 nodes, FA_8 was detected at the N. Ferulates were also detected in a previous study. The $H_{2/6}$ signals could be detected at both RG1-N and RG1-IN, but the FA8 substructures were not observed.

To understand the lignin compositional variation across the variety and growing seasons, the volume integration method was used to determine the relative abundances of the S and G lignin units (S/G ratio). Thus, the average S/G ratios in D1, RG1, D2, and RG2 were about 0.40, 0.51, 0.43, and 0.62, respectively. For energy sorghum the S/G ratio of 0.53-0.58 was reported by McKinley et al. 32 while a S/G ratio of 0.4 was obtained for sugarcane straw. 87 The S/G ratio for RG was significantly higher than Della in both growing seasons, which is consistent with the FTIR and Py-GCMS results. Besides demonstrating G-rich lignin in sorghum stalks, the result also indicates that the Della variety contains less S lignin than RG, which reveals the alteration of lignin composition. Although HSQC NMR is an entirely nonquantitative technique, the S/G ratio by this method is considered relatively reliable.⁸⁸ Contrarily, the pCA and FA units are significantly overestimated due to the longer relaxation of more mobile units than the backbone units in the cell wall.⁵⁵ Hence, quantification of FA and pCA units from the volume integrals was not considered. Across the growing seasons, the S/G ratio of D1 and D2 was approximately equivalent, but RG2 was higher than RG1.

In summary, the structural carbohydrate, lignin compositional and structural variations in the cell wall of RG and Della sorghum stalks has been determined and this could provide insights of their biomechanical strength. The significant variations in the glucan, xylan, and lignin contents may result in disparity in the mechanical behavior of the stalk. Furthermore, structural and compositional features of cellulose and lignin (e.g., CI, S/G ratios) and the occurrence of different extents of nonacylated and naturally γ -acylated β -O-4

substructures may have different effects on the stiffness of the stalks. A future study will evaluate the impact of structural carbohydrates and lignin on the mechanical strength of the stalks and the correlating cell wall compositional and structural differences in RG and Della with their corresponding biomechanical strength.

ASSOCIATED CONTENT

Solution Supporting Information

The Supporting Information is available free of charge at https://pubs.acs.org/doi/10.1021/acs.jafc.1c07176.

FTIR assignments for main functional groups in sorghum stalk biomass assigned based on the literature 44,46,47 (Table S1); identification and relative abundance (%) of main pyrolysates from internodes of D1, RG1, D2, and RG2 sorghum stalks (Table S2); compounds identified and relative abundance (area %) of pyrolysates from nodes of D1, RG1, D2, and RG2 stalks (Table S3); HSQC assignments of sorghum stalk whole-cell wall in the DMSO- d_6 /pyridine- d_5 solvent (Table S4); GCMS pyrogram of sorghum stalks D2-IN, RG2-IN, D1-IN, and RG1-IN (Figure S1); Py-GCMS pyrogram of sorghum stalks D2-N, RG2-N, D1-N, and RG1-N (Figure S2); HSQC of sorghum whole-cell wall gels in DMSO- d_6 /pyridine- d_5 (4:1) solvent in the aromatic region at nodes (N) D1-N, RG1-N, D2-N, and RG2-N (Figure S3); and basic lignin structures (Figure S4) (PDF)

AUTHOR INFORMATION

Corresponding Author

Armando G. McDonald — Renewable Materials Program, Department of Forest, Rangeland and Fire Sciences, University of Idaho, Moscow, Idaho 83844-1132, United States; Email: armandm@uidaho.edu

Authors

Endalkachew Mengistie — Renewable Materials Program, Department of Forest, Rangeland and Fire Sciences, University of Idaho, Moscow, Idaho 83844-1132, United States

Abdulbaset M. Alayat – Renewable Materials Program, Department of Forest, Rangeland and Fire Sciences, University of Idaho, Moscow, Idaho 83844-1132, United States

Farid Sotoudehnia — Renewable Materials Program, Department of Forest, Rangeland and Fire Sciences, University of Idaho, Moscow, Idaho 83844-1132, United States

Norbert Bokros – Plant Physiology, Department of Horticulture, Agricultural Science Center North, University of Kentucky, Lexington, Kentucky 40546, United States

Seth DeBolt – Plant Physiology, Department of Horticulture, Agricultural Science Center North, University of Kentucky, Lexington, Kentucky 40546, United States

Complete contact information is available at: https://pubs.acs.org/10.1021/acs.jafc.1c07176

Notes

The authors declare no competing financial interest.

ACKNOWLEDGMENTS

The authors would like to acknowledge (i) the financial support from the National Science Foundation, Grant # 1826715, (ii) the University of Idaho Equipment and Infrastructure Support (EIS) Awards Program from the Office of Research and Economic Development (ORED) RISE Funding Program and the College of Natural Resources for supporting the purchase of the GCMS, (iii) Dr. Thomas Williams for performing the XRD analyses, and (iv) The M. J. Murdock Charitable Trust, Vancouver, WA, Reference No.: 2014120:MNL:11/20/2014, for supporting the purchase of the NMR spectrometer.

REFERENCES

- (1) Xia, J.; Zhao, Y.; Burks, P.; Pauly, M.; Brown, P. J. A sorghum NAC gene is associated with variation in biomass properties and yield potential. *Plant Direct* **2018**, *2*, No. e00070.
- (2) Bakeer, B.; Taha, I.; El-Mously, H.; Shehata, S. On the characterisation of structure and properties of sorghum stalks. *Ain Shams Eng. J.* **2013**, *4*, 265–271.
- (3) Cook, D. D.; et al. Stalk Lodging: A Portable Device for Phenotyping Stalk Bending Strength of Maize and Sorghum. *bioRxiv* **2019**, No. 567578.
- (4) Berry, P.; Spink, J. Predicting yield losses caused by lodging in wheat. Field Crops Res. 2012, 137, 19–26.
- (5) Davison, B. H.; Parks, J.; Davis, M. F.; Donohoe, B. S. Plant Cell Walls: Basics of Structure, Chemistry, Accessibility and the Influence on Conversion. In Aqueous Pretreatment of Plant Biomass for Biological and Chemical Conversion to Fuels and Chemicals; Wyman, C. E., Ed.; John Wiley & Sons, Ltd., 2013; pp 23–38.
- (6) Liao, J. J.; Latif, N. H. A.; Trache, D.; Brosse, N.; Hussin, M. H. Current advancement on the isolation, characterization and application of lignin. *Int. J. Biol. Macromol.* **2020**, *162*, 985–1024.
- (7) Rongpipi, S.; Ye, D.; Gomez, E. D.; Gomez, E. W. Progress and Opportunities in the Characterization of Cellulose An Important Regulator of Cell Wall Growth and Mechanics. *Front. Plant Sci.* **2019**, 9, No. 1894.
- (8) Cosgrove, D. J.; Jarvis, M. Comparative structure and biomechanics of plant primary and secondary cell walls. *Front. Plant Sci.* **2012**, *3*, No. 204.
- (9) Wang, J.; Zhu, J.; Huang, R.; Yang, Y. Investigation of cell wall composition related to stem lodging resistance in wheat (*Triticum aestivum* L.) by FTIR spectroscopy. *Plant Signaling Behav.* **2012**, *7*, 856–863.
- (10) Sekhon, R. S.; et al. Stalk Bending Strength is Strongly Associated with Maize Stalk Lodging Incidence Across Multiple Environments. *Field Crops Res.* **2020**, 249, No. 107737.
- (11) Berry, P.; et al. Understanding and Reducing Lodging in Cereals. Adv. Agron. 2004, 84, 217–271.
- (12) Liu, Q.; Luo, L.; Zheng, L. Lignins: Biosynthesis and Biological Functions in Plants. *Int. J. Mol. Sci.* **2018**, *19*, No. 335.
- (13) Xiang, D.; et al. Relationship between stem characteristics and lodging resistance of Tartary buckwheat (*Fagopyrum tataricum*). *Plant Prod. Sci.* **2019**, 22, 202–210.
- (14) Li, M.; Pu, Y.; Ragauskas, A. J. Current Understanding of the Correlation of Lignin Structure with Biomass Recalcitrance. *Front. Chem.* **2016**, *4*, No. 45.
- (15) Sattler, S. E.; et al. Characterization of Novel Sorghum brown midrib Mutants from an EMS-Mutagenized Population. G3 GenesGenomesGenetics 2014, 4, 2115–2124.
- (16) Petti, C.; et al. Sorghum mutant RGdisplays antithetic leaf shoot lignin accumulation resulting in improved stem saccharification properties. *Biotechnol. Biofuels* **2013**, *6*, No. 146.
- (17) Vogler, H.; Felekis, D.; Nelson, B. J.; Grossniklaus, U. Measuring the Mechanical Properties of Plant Cell Walls. *Plants* **2015**, *4*, 167–182.

- (18) Mengistie, E.; et al. Fatty Acid Profile-Based Chemometrics to Differentiate Metabolic Variations in Sorghum. *ACS Food Sci. Technol.* **2021**, *1*, 2127–2134.
- (19) Santos, J.; et al. Lignin-enriched Fermentation Residues from Bioethanol Production of Fast-growing Poplar and Forage Sorghum. *BioResources* **2015**, *10*, 5215–5232.
- (20) Kline, L.; Hayes, D.; Womac, A.; Labbé, N. Simplified determination of lignin content in hard and soft woods via UV-spectrophotometric analysis of biomass dissolved in ionic liquids. *BioResources* **2010**, *5*, 1366–1383.
- (21) Balogun, A. O.; McDonald, A. G. Decomposition kinetic study, spectroscopic and pyrolytic analyses of Isoberlinia doka and Pinus ponderosa. *Biomass Convers. Biorefin.* **2016**, *6*, 315–324.
- (22) Hurtubise, F. G.; Krassig, H. Classification of Fine Structural Characteristics in Cellulose by Infared Spectroscopy. Use of Potassium Bromide Pellet Technique. *Anal. Chem.* **1960**, 32, 177–181.
- (23) Faix, O.; Meier, D.; Fortmann, I. Thermal degradation products of wood. *Holz Roh- Werkst.* **1990**, *48*, 351–354.
- (24) Faix, O.; Fortmann, I.; Bremer, J.; Meier, D. Thermal degradation products of wood. *Holz Roh- Werkst.* **1991**, 49, 213–219.
- (25) Meier, D.; Faix, O. Pyrolysis-Gas Chromatography-Mass Spectrometry. In *Methods in Lignin Chemistry*; Lin, S. Y.; Dence, C. W., Eds.; Springer, 1992; pp 177–199.
- (26) Poletto, M.; Ornaghi, H.; Zattera, A. Native Cellulose: Structure, Characterization and Thermal Properties. *Materials* **2014**, 7, 6105–6119.
- (27) Segal, L.; Creely, J. J.; Martin, A. E.; Conrad, C. M. An Empirical Method for Estimating the Degree of Crystallinity of Native Cellulose Using the X-Ray Diffractometer. *Text. Res. J.* **1959**, *29*, 786–794
- (28) French, A. D.; Santiago Cintrón, M. Cellulose polymorphy, crystallite size, and the Segal Crystallinity Index. *Cellulose* **2013**, *20*, 583–588
- (29) Kim, H.; Ralph, J. Solution-state 2D NMR of ball-milled plant cell wall gels in DMSO-d6/pyridine-d5. *Org. Biomol. Chem.* **2010**, *8*, 576–591.
- (30) Byrt, C. S.; et al. Prospecting for Energy-Rich Renewable Raw Materials: Sorghum Stem Case Study. *PLoS One* **2016**, *11*, No. e0156638.
- (31) Petti, C.; et al. Comparative feedstock analysis in *Setaria viridis* L. as a model for C4 bioenergy grasses and Panicoid crop species. *Front. Plant Sci.* **2013**, *4*, No. 181.
- (32) McKinley, B. A.; et al. Variation in energy sorghum hybrid TX08001 biomass composition and lignin chemistry during development under irrigated and non-irrigated field conditions. *PLoS One* **2018**, *13*, No. e0195863.
- (33) Patton, A. R.; Gieseker, L. Seasonal Changes in the Lignin and Cellulose Content of Some Montana Grasses. *J. Anim. Sci.* **1942**, *1*, 22–26.
- (34) Mann, D. G. J.; et al. Rapid Assessment of Lignin Content and Structure in Switchgrass (*Panicum virgatum* L.) Grown Under Different Environmental Conditions. *BioEnergy Res.* **2009**, 2, 246–256.
- (35) Gomez, F. E.; Muliana, A. H.; Niklas, K. J.; Rooney, W. L. Identifying Morphological and Mechanical Traits Associated with Stem Lodging in Bioenergy Sorghum (*Sorghum bicolor*). *BioEnergy Res.* **2017**, *10*, 635–647.
- (36) Yuan, T.-Q.; Sun, S.-N.; Xu, F.; Sun, R.-C. Characterization of Lignin Structures and Lignin—Carbohydrate Complex (LCC) Linkages by Quantitative 13C and 2D HSQC NMR Spectroscopy. *J. Agric. Food Chem.* **2011**, *59*, 10604–10614.
- (37) Wang, B.; Smith, S. M.; Li, J. Genetic Regulation of Shoot Architecture. *Annu. Rev. Plant Biol.* **2018**, *69*, 437–468.
- (38) Gao, Y.; Lipton, A. S.; Wittmer, Y.; Murray, D. T.; Mortimer, J. C. A grass-specific cellulose—xylan interaction dominates in sorghum secondary cell walls. *Nat. Commun.* **2020**, *11*, No. 6081.
- (39) Novaes, E.; Kirst, M.; Chiang, V.; Winter-Sederoff, H.; Sederoff, R. Lignin and Biomass: A Negative Correlation for Wood

- Formation and Lignin Content in Trees1. *Plant Physiol.* **2010**, *154*, 555–561.
- (40) Hatfield, R. D.; Wilson, J. R.; Mertens, D. R. Composition of cell walls isolated from cell types of grain sorghum stems. *J. Sci. Food Agric.* **1999**, *79*, 891–899.
- (41) Petti, C.; Hirano, K.; Stork, J.; DeBolt, S. Mapping of a Cellulose-Deficient Mutant Named dwarf1-1 in *Sorghum bicolor* to the Green Revolution Gene gibberellin20-oxidase Reveals a Positive Regulatory Association between Gibberellin and Cellulose Biosynthesis. *Plant Physiol.* **2015**, *169*, 705–716.
- (42) Richie, W. R.; McBee, G. G. Structural components in Sorghum stem biomass. *Bioresour. Technol.* **1991**, *38*, 15–22.
- (43) Billa, E.; Koullas, D. P.; Monties, B.; Koukios, E. G. Structure and composition of sweet sorghum stalk components. *Ind. Crops Prod.* **1997**, *6*, 297–302.
- (44) Ghaffar, S. H.; Fan, M. Revealing the morphology and chemical distribution of nodes in wheat straw. *Biomass Bioenergy* **2015**, *77*, 123–134.
- (45) Corredor, D. Y.; et al. Evaluation and Characterization of Forage Sorghum as Feedstock for Fermentable Sugar Production. *Appl. Biochem. Biotechnol.* **2009**, 158, 164–179.
- (46) Stark, N. M.; Yelle, D. J.; Agarwal, U. P. Techniques for Characterizing Lignin. *Lignin in Polymer Composites*; Elsevier, 2016; pp 49–66.
- (47) Faix, O. Classification of Lignins from Different Botanical Origins by FT-IR Spectroscopy. *Holzforschung* **1991**, *45*, 21–28.
- (48) Liu, C.; Wang, X.; Lin, F.; Zhang, H.; Xiao, R. Structural elucidation of industrial bioethanol residual lignin from corn stalk: A potential source of vinyl phenolics. *Fuel Process. Technol.* **2018**, *169*, 50–57.
- (49) Boukir, A.; Fellak, S.; Doumenq, P. Structural characterization of Argania spinosa Moroccan wooden artifacts during natural degradation progress using infrared spectroscopy (ATR-FTIR) and X-Ray diffraction (XRD). *Heliyon* **2019**, *5*, No. e02477.
- (50) Safou-Tchiama, R.; Barhé, T.; Soulounganga, P.; Akagah, A.; Jeso, B. A comparative study of the syringyl, guaiacyl and hydroxyl groups units distribution in some African tropical hardwoods' lignin by Py-GC/MS and spectroscopic techniques. *J. Mater. Environ. Sci.* **2016**, *8*, 2530–2540.
- (51) Nelson, M. L.; O'Connor, R. T. Relation of certain infrared bands to cellulose crystallinity and crystal latticed type. Part I. Spectra of lattice types I, II, III and of amorphous cellulose. *J. Appl. Polym. Sci.* **1964**, *8*, 1311–1324.
- (52) Sammons, R.; et al. Characterization of Organosolv Lignins using Thermal and FT-IR Spectroscopic Analysis. *BioResources* **2013**, 8, 2752.
- (53) Ziebell, A.; et al. Increase in 4-Coumaryl Alcohol Units during Lignification in Alfalfa (*Medicago sativa*) Alters the Extractability and Molecular Weight of Lignin. *J. Biol. Chem.* **2010**, 285, 38961–38968.
- (54) Hoffmann, A.; Bremer, M.; Fischer, S. Determination of Monomeric Building Blocks by Py-GC/MS of Lignins from Agricultural Residues. *Austin Biomol.* **2019**, *3*, No. 1013.
- (55) del Río, J. C.; et al. Structural Characterization of Wheat Straw Lignin as Revealed by Analytical Pyrolysis, 2D-NMR, and Reductive Cleavage Methods. *J. Agric. Food Chem.* **2012**, *60*, 5922–5935.
- (56) del Río, J. C.; et al. Structural Characterization of the Lignin in the Cortex and Pith of Elephant Grass (*Pennisetum purpureum*) Stems. *J. Agric. Food Chem.* **2012**, *60*, 3619–3634.
- (57) Van Kuijk, S. J. A.; et al. Selective ligninolysis of wheat straw and wood chips by the white-rot fungus *Lentinula edodes* and its influence on in vitro rumen degradability. *J. Anim. Sci. Biotechnol.* **2016**, 7, No. 55.
- (58) Olsson, A.-M.; Salmén, L. The effect of lignin structure on the viscoelastic properties of wood. *Nord. Pulp Pap. Res. J.* **1997**, *12*, 140–144.
- (59) Wei, L.; et al. Genetic and transcriptomic analyses of lignin- and lodging-related traits in Brassica napus. *Theor. Appl. Genet.* **2017**, *130*, 1961–1973.

- (60) Lupoi, J. S.; Singh, S.; Simmons, B. A.; Henry, R. J. Assessment of Lignocellulosic Biomass Using Analytical Spectroscopy: an Evolution to High-Throughput Techniques. *BioEnergy Res.* **2014**, *7*, 1–23.
- (61) Yan, J.; Hu, Z.; Pu, Y.; Charles Brummer, E.; Ragauskas, A. J. Chemical compositions of four switchgrass populations. *Biomass Bioenergy* **2010**, *34*, 48–53.
- (62) El Hage, R.; et al. Characterization of milled wood lignin and ethanol organosolv lignin from miscanthus. *Polym. Degrad. Stab.* **2009**, 94, 1632–1638.
- (63) Van Erven, G.; et al. Quantification of Lignin and Its Structural Features in Plant Biomass Using 13C Lignin as Internal Standard for Pyrolysis-GC-SIM-MS. *Anal. Chem.* **2017**, *89*, 10907–10916.
- (64) Lourenço, A.; et al. Lignin Composition and Structure Differs between Xylem, Phloem and Phellem in *Quercus suber L. Front. Plant Sci.* **2016**, 7, No. 1612.
- (65) Carrier, M.; et al. Thermogravimetric analysis as a new method to determine the lignocellulosic composition of biomass. *Biomass Bioenergy* **2011**, *35*, 298–307.
- (66) Lv, G.; Wu, S. Analytical pyrolysis studies of corn stalk and its three main components by TG-MS and Py-GC/MS. *J. Anal. Appl. Pyrolysis* **2012**, *97*, 11–18.
- (67) Wang, T.; Yin, J.; Liu, Y.; Lu, Q.; Zheng, Z. Effects of chemical inhomogeneity on pyrolysis behaviors of corn stalk fractions. *Fuel* **2014**, *129*, 111–115.
- (68) Burhenne, L.; Messmer, J.; Aicher, T.; Laborie, M.-P. The effect of the biomass components lignin, cellulose and hemicellulose on TGA and fixed bed pyrolysis. *J. Anal. Appl. Pyrolysis* **2013**, *101*, 177–184
- (69) Brebu, M.; Vasile, C. Thermal degradation of lignin A Review. *Cellul. Chem. Technol.* **2010**, *44*, 353–363.
- (70) Huang, S.; Wu, Q.; Zhou, D.; Huang, R. Thermal Decomposition Properties of Materials from Different Parts of Corn Stalk. *BioResources* **2015**, *10*, 2020–2031.
- (71) Watkins, D.; Nuruddin, M.; Hosur, M.; Tcherbi-Narteh, A.; Jeelani, S. Extraction and characterization of lignin from different biomass resources. *J. Mater. Res. Technol.* **2015**, *4*, 26–32.
- (72) Agarwal, U. P.; Ralph, S. A.; Reiner, R. S.; Baez, C. Probing crystallinity of never-dried wood cellulose with Raman spectroscopy. *Cellulose* **2016**, 23, 125–144.
- (73) Agarwal, U. P.; Ralph, S. A.; Reiner, R. S.; Baez, C. New cellulose crystallinity estimation method that differentiates between organized and crystalline phases. *Carbohydr. Polym.* **2018**, *190*, 262–270.
- (74) Agarwal, U. P.; Ralph, S. A.; Baez, C.; Reiner, R. S. Contributions of Crystalline and Noncrystalline Cellulose Can Occur in the Same Spectral Regions: Evidence Based on Raman and IR and Its Implication for Crystallinity Measurements. *Biomacromolecules* **2021**, 22, 1357–1373.
- (75) Kim, H.; Ralph, J. A gel-state 2D-NMR method for plant cell wall profiling and analysis: a model study with the amorphous cellulose and xylan from ball-milled cotton linters. *RSC Adv.* **2014**, *4*, 7549–7560.
- (76) Balakshin, M.; Capanema, E.; Gracz, H.; Chang, H.; Jameel, H. Quantification of lignin-carbohydrate linkages with high-resolution NMR spectroscopy. *Planta* **2011**, 233, 1097–1110.
- (77) Komatsu, T.; Kikuchi, J. Comprehensive Signal Assignment of ¹³ C-Labeled Lignocellulose Using Multidimensional Solution NMR and ¹³ C Chemical Shift Comparison with Solid-State NMR. *Anal. Chem.* **2013**, 85, 8857–8865.
- (78) Rencoret, J.; et al. HSQC-NMR analysis of lignin in woody (*Eucalyptus globulus* and *Picea abies*) and non-woody (*Agave sisalana*) ball-milled plant materials at the gel state 10th EWLP, Stockholm, Sweden, August 25–28, 2008. *Holzforschung* **2009**, *63*, *691*.
- (79) Mansfield, S. D.; Kim, H.; Lu, F.; Ralph, J. Whole plant cell wall characterization using solution-state 2D NMR. *Nat. Protoc.* **2012**, *7*, 1579–1589.

- (80) Samuel, R.; et al. Structural Characterization of Lignin in Wild-Type versus COMT Down-Regulated Switchgrass. *Front. Energy Res.* **2014**, *1*, No. 14.
- (81) Komatsu, T.; Kikuchi, J. Comprehensive Signal Assignment of 13C-Labeled Lignocellulose Using Multidimensional Solution NMR and 13C Chemical Shift Comparison with Solid-State NMR. *Anal. Chem.* **2013**, *85*, 8857–8865.
- (82) Rencoret, J.; et al. Variability in Lignin Composition and Structure in Cell Walls of Different Parts of Macaúba (*Acrocomia aculeata*) Palm Fruit. *J. Agric. Food Chem.* **2018**, *66*, 138–153.
- (83) del Río, J. C.; et al. Highly Acylated (Acetylated and/or p-Coumaroylated) Native Lignins from Diverse Herbaceous Plants. *J. Agric. Food Chem.* **2008**, *56*, 9525–9534.
- (84) Anderson, N. A.; et al. Manipulation of Guaiacyl and Syringyl Monomer Biosynthesis in an Arabidopsis Cinnamyl Alcohol Dehydrogenase Mutant Results in Atypical Lignin Biosynthesis and Modified Cell Wall Structure. *Plant Cell* **2015**, *27*, 2195–2209.
- (85) Fornalé, S.; et al. Changes in Cell Wall Polymers and Degradability in Maize Mutants Lacking 3'- and 5'-O-Methyltransferases Involved in Lignin Biosynthesis. *Plant Cell Physiol.* **2017**, 58, 240–255.
- (86) Eudes, A.; et al. SbCOMT (Bmr12) is involved in the biosynthesis of tricin-lignin in sorghum. *PLoS One* **2017**, *12*, No. e0178160.
- (87) del Río, J. C.; et al. Differences in the chemical structure of the lignins from sugarcane bagasse and straw. *Biomass Bioenergy* **2015**, *81*, 322–338.
- (88) Wen, J.-L.; Sun, S.-L.; Xue, B.-L.; Sun, R.-C. Recent Advances in Characterization of Lignin Polymer by Solution-State Nuclear Magnetic Resonance (NMR) Methodology. *Materials* **2013**, *6*, 359–391.

